GRACE satellite observations of Antarctic Bottom Water transport variability

Jemma Jeffree[1,2], Andrew McC. Hogg[1,2], Adele K. Morrison[1,2,3], Aviv Solodoch[4], Andrew L. Stewart[5], Rebecca McGirr[1,3]

[1]Research School of Earth Sciences, Australian National University, Canberra, ACT, Australia
[2]ARC Centre of Excellence for Climate Extremes, Australia
[3]The Australian Centre for Excellence in Antarctic Science, University of Tasmania, Hobart, Tasmania, Australia
[4]Institute of Earth Sciences, Hebrew University of Jerusalem, Jerusalem, Israel
[5]Department of Atmospheric and Oceanic Sciences, University of California, Los Angeles, CA 90095, USA

Key Points:

- We use estimates of ocean bottom pressure from the GRACE satellites as a proxy for Antarctic Bottom Water transport
- The largest source of uncertainty in our reconstruction is satellite measurement uncertainty
- We reconstruct Antarctic Bottom Water transport anomalies, capturing an estimated 50% of variance

Corresponding author: Jemma Jeffree, jemma.jeffree@anu.edu.au

Abstract

Antarctic Bottom Water (AABW) formation and transport constitute a key component of the global ocean circulation. Direct observations suggest that AABW volumes and transport rates may be decreasing, but these observations are too temporally or spatially sparse to determine the cause. To address this problem, we develop a new method to reconstruct AABW transport variability using data from the GRACE (Gravity Recovery and Climate Experiment) satellite mission. We use an ocean general circulation model to investigate the relationship between ocean bottom pressure and AABW: we calculate both of these quantities in the model, and link them using a regularised linear regression. Our reconstruction from modelled ocean bottom pressure can capture 65-90% of modelled AABW transport variability, depending on the ocean basin. When realistic observational uncertainty values are added to the modelled ocean bottom pressure, the reconstruction can still capture 30-80% of AABW transport variability. Using the same regression values, the reconstruction skill is within the same range in a second, independent, general circulation model. We conclude that our reconstruction method is not unique to the model in which it was developed and can be applied to GRACE satellite observations of ocean bottom pressure. These advances allow us to create the first global reconstruction of AABW transport variability over the satellite era. Our reconstruction provides information on the interannual variability of AABW transport, but more accurate observations are needed to discern AABW transport trends.

Plain Language Summary

Ocean circulation moves heat and carbon around the globe. Changes in the way this circulation moves heat and carbon influence future climate. One part of this ocean circulation is Antarctic Bottom Water, which forms around Antarctica and flows north along the ocean floor into the Pacific, Atlantic and Indian Oceans. Observations of Antarctic Bottom Water are sparse. Those which exist suggest that the volume of Antarctic Bottom Water is declining, but are insufficient to explain why this is happening.

We design a new method to try and measure Antarctic Bottom Water transport. The physical equations describing fluid flows suggest gravity signals measured by satellites might be useful. To establish how useful this data is, we simulate the observations of these satellites in an ocean model. We also calculate the transport of Antarctic Bottom Water in the model. This means we can investigate how effective the modelled satel-

lite data is at measuring modelled Antarctic Bottom Water. Our method of using the satellite data skilfully measures Antarctic Bottom Water transport, so we use this method to calculate Antarctic Bottom Water from the real-world satellite observations.

1 Introduction

The lower limb of the global meridional overturning circulation is composed of Antarctic Bottom Water (AABW). AABW is a dense watermass that forms near Antarctica and flows northwards along the ocean floor in the Pacific, Indian and Atlantic Oceans (Talley, 2013). AABW composes a third of the ocean volume, and covers more than half the ocean floor (Johnson, 2008).

Observations of AABW provide some information about the mean flow and characteristics of this water mass. Temperature and salinity profiles along research vessel transects have been gathered by the WOCE and GOSHIP programs roughly once per decade. These transects are temporally sparse compared to the timescales on which AABW transport varies (Purkey & Johnson, 2012; Stewart et al., 2021). Localised mooring arrays have provided information with daily resolution, but only sample a subset of AABW pathways (e.g. Fukamachi et al., 2010; Valla et al., 2019). More recently, deep Argo floats have expanded knowledge of AABW in specific areas (e.g. Foppert et al., 2021; Johnson, 2022). Although deep Argo floats will give more information in the future, their collected data currently comprises only several years, and over a relatively small fraction of the Southern Ocean. As such, there is no source of AABW observations with sufficient spatial and temporal coverage to constrain the variability of AABW transport.

Higher resolution observations of AABW could improve understanding of its response to climate change. Recent modelling work suggests a halving of AABW production and transport by 2050 in response to projected Antarctic meltwater forcing (Li et al., 2023). Observations also show that the volume of AABW has declined in recent decades (Purkey & Johnson, 2012). Recent studies associate this reduction in Bottom Water volume with declining production of the precursor Dense Shelf Water, but note that data limitations prevent direct observations of this link (Abrahamsen et al., 2019; Zhou et al., 2023). Furthermore, natural variability in AABW can produce apparent trends without the aid of external forcing (Zhang et al., 2019). Further investigation into the tem-

poral variability of AABW would shed light on how AABW transport and other related processes are changing.

One option to supplement *in-situ* observations of AABW is satellite data. Satellite measurements of horizontal ocean pressure gradients indirectly measure geostrophic ocean transport. This link has been utilised to estimate ocean transport in the upper 1000m of the ocean from satellite altimetry of sea surface height gradients, with some correction due to steric variability (e.g. Ivchenko et al., 2011; Kosempa & Chambers, 2014). However, deep baroclinic flows are less directly related to surface pressure gradients, and deep density observations are too sparse to correct for this. Deep geostrophic flows can instead be inferred from ocean bottom pressure (Hughes et al., 2013), which is measured by the GRACE (Gravity Recovery and Climate Experiment) satellites. In practice, in the ECCO ocean state estimate, almost all (95%) AABW transport at any latitude in the Southern Ocean can be reconstructed from ocean bottom pressure using a neural network (Solodoch et al., 2023), demonstrating that sufficiently accurate and high resolution observations of ocean bottom pressure can be used alone to reconstruct AABW transport.

The GRACE satellites measure mass anomalies on Earth's surface. These mass anomalies correspond, via hydrostatic balance, to ocean bottom pressure anomalies, which suggests that the GRACE satellite observations could be used to infer AABW transport anomalies. However, both the resolution and accuracy of GRACE satellite observations of ocean bottom pressure limit their potential to reconstruct AABW transport. For example, the standard error of GRACE satellite estimates of ocean bottom pressure is 10^{-2} dbar (Watkins et al., 2015), around the same magnitude as ocean bottom pressure variability (Poropat et al., 2018). The coarse spatial resolution of GRACE-derived outputs ($\sim$300 km), combines ocean bottom pressure signals from different depths on the continental slope and thus could conflate estimates of ocean transport at different depths (Hughes et al., 2018). Bingham and Hughes (2008) suggested that that the depth-dependent part of ocean bottom pressure anomalies are key to estimating ocean transport.

However, case studies of North Atlantic Deep Water (NADW; a similar water mass to AABW) suggest that satellite-derived ocean bottom pressure can reconstruct ocean transport despite these barriers. Bentel et al. (2015) found that ocean bottom pressure in a model, coarsened to the the same $\sim$300 km grid as GRACE satellite observations,

could reconstruct the model's NADW with a correlation coefficient of 0.7. Landerer et al. (2015) later compared a reconstruction of NADW from GRACE satellite estimates with estimates from an *in-situ* mooring array, finding a similar correlation coefficient. Therefore, although GRACE satellite estimates of ocean bottom pressure are at lower resolution and higher uncertainty than model output, they remain a viable proxy for deep ocean transport in the North Atlantic.

In the Southern Hemisphere, only one study has used satellite estimates of ocean bottom pressure to reconstruct AABW transport, and no study has done so comprehensively. Mazloff and Boening (2016) focused on a specific region of the Pacific Ocean, and found that ocean bottom pressure can reconstruct 86% of AABW transport variance in this region. They gave an estimate of how GRACE satellite estimates of ocean bottom pressure might be used to reconstruct AABW. However, Mazloff and Boening (2016) only looked at one region, and their uncertainty estimation hinged on a comparison with a single *in-situ* location. No satellite-based basin-wide estimates of AABW transport exist. Additionally, no previous work has considered together the impacts of resolution and uncertainty when using GRACE observations to reconstruct AABW.

In this paper we quantify the accuracy that satellite observations of ocean bottom pressure can provide for estimation of AABW transport variability. We develop a simple empirical method to link modelled ocean bottom pressure with AABW transport (Section 2). This method is tested on AABW transport in a high-resolution ocean model, where the ocean bottom pressure observations are degraded by coarsening resolution and adding noise to emulate the characteristics of satellite observations (Section 3). We then apply this method to GRACE satellite observations of ocean bottom pressure, to estimate the interannual variability in AABW transport (Section 4).

2 Reconstruction Method

We aim to develop a method to reconstruct AABW transport from GRACE satellite observations of ocean bottom pressure, and to quantify the performance of this method. There are insufficient *in-situ* AABW transport observations against which to test the accuracy of the reconstruction method, so we develop and test our method using output from an ocean general circulation model. We take both AABW transport and ocean bottom pressure from the ocean model output, and link these variables with a multivari-

ate linear regression. This reconstruction method can then be applied to ocean bottom pressure from another numerical model, to test the reconstruction method's generality, and to satellite observations of ocean bottom pressure, to produce an estimate of AABW transport variability.

2.1 Ocean Model

We develop our reconstruction method using output from ACCESS-OM2-01, a coupled sea-ice/ocean model with prescribed atmospheric forcing. The model uses a 0.1° Mercator grid; full model configuration is described in Kiss et al. (2020). ACCESS-OM2-01 is one of the few models which adequately represents AABW sourced from dense water formed on the Antarctic continental shelf, instead of in the open ocean (Solodoch et al., 2022). Additionally, the high resolution allows ACCESS-OM2-01 to represent eddies and other mesoscale structures over much of the globe without parameterisation. By accurately representing more ocean processes, ACCESS-OM2-01 is more likely to correctly represent links between AABW transport and ocean bottom pressure.

We use model output from two model runs of ACCESS-OM2-01, with different prescribed atmospheric forcing. One model run uses atmospheric forcing from the JRA55-do reanalysis dataset from January 1958 to December 2018 (Tsujino et al., 2018). We term this the historically forced model run. The other model run uses a continuous cycling of the May 1990 to April 1991 atmosphere from JRA55-do (Stewart et al., 2021), for which we have 230 years of monthly data. We term this the repeat year forced model run. These two model runs provide a combined total of 291 years of data.

Our multivariate linear regression model is fitted to, or trained on, the repeat-year forced ACCESS-OM2-01 data. We initially test our method, and empirically refine methodology, on the historical run of ACCESS-OM2-01. In addition, we test the generalisability of our method, trained on ACCESS-OM2-01 output, with the output from two additional models: a historically forced run of ACCESS-OM2 at 0.25° resolution (ACCESS-OM2-025; Kiss et al., 2020) and a repeat year forced run of GFDL-OM4 at 0.25° resolution (GFDL-OM4-025; Adcroft et al., 2019). Output from these models is arguably more independent of the training data than output from a separate run of ACCESS-OM2-01, and so testing our method on output from these different models increases confidence in the estimate of our method uncertainty.

2.2 AABW transport definition

In this paper we define AABW, in each ocean basin, to be water denser than a particular density threshold. At a given latitude, the monthly AABW transport (ψ_t) below the isopycnal ρ_1 at time t is given by

$$\psi_t(\rho_1) = \int_{x_0}^{x_1} \int_{z_0}^{z_t(\rho_1)} v_t dz dx \tag{1}$$

where x_0, x_1 are the longitudinal bounds of a transect, z_0 is the height of the ocean floor, $z_t(\rho_1)$ is the height of the density threshold ρ_1 at time t, and v_t is the meridional velocity at time t. Meridional transport in density coordinates is a supplied diagnostic in the ACCESS-OM2-01 runs, but at insufficiently high resolution at AABW depths. Instead, we bin meridional transport into density bins at 0.01 kgm^{-3} spacing over the range 1036.5–1037.5 kgm^{-3} using monthly output. The use of monthly averaged density and velocity may omit eddy contributions to transport magnitude; we find that this omission is not significant at the latitudes tested here. The correlation between 12 months of AABW transport calculated using monthly or daily data is $\geq$0.98 in each basin (not shown). The mean ACCESS-OM2-01 AABW transport across 30°S from the historically forced model run is 18.5 Sv (10^6m^{3}s^{-1}), the same order of magnitude as estimates from observations, which range from 10 Sv to 50 Sv (Sloyan & Rintoul, 2001; Lumpkin & Speer, 2007; Talley, 2013).

For each model, at any given latitude, we define the AABW threshold to be the isopycnal bounding northward flowing water at the ocean bottom. The one exception to this definition is in GFDL-OM4 in the Pacific Ocean, where we overwrite the density threshold with that from ACCESS-OM2-01, because our streamfunction definition produces unrealistic AABW transport (details in Text S1 and Figure S1). We reconstruct AABW at 30°S in the Atlantic and Indian Oceans, and 40°S in the Pacific Ocean, because these latitudes maximise the skill of our AABW reconstruction (See Section 2.6 and Figure S5). The attributes of ACCESS-OM2-01 AABW calculated following this method are shown in Table 1.

2.3 Building a Linear Regression Model for AABW Transport

Ocean bottom pressure gradients along an ocean cross section are linearly related to large-scale ocean transport through that cross section, including AABW transport (Hughes et al., 2013). This physical link could be used to directly estimate AABW transport from

Table 1. AABW transport and the definition of AABW in each ocean basin, used to train and test the regression in ACCESS-OM2-01. The latitudes are chosen separately in each ocean basin in order to maximise reconstruction skill (See Section 2.6 and Figure S5).

Ocean	Latitude	Potential density (σ_2) threshold	Mean transport
Pacific	40°S	1037.08 kgm^{-3}	10.2 Sv
Atlantic	30°S	1037.08 kgm^{-3}	4.6 Sv
Indian	30°S	1037.09 kgm^{-3}	3.8 Sv

ocean bottom pressure, in the same way that Landerer et al. (2015) reconstructed NADW. However, such an approach limits the ocean bottom pressure to that along a single line of latitude, even though ocean bottom pressure to the north and south of a zonal transect correlates with transport across the transect (Landerer et al., 2015). Solodoch et al. (2023) found meridional averaging didn't affect reconstruction skill in a noise-free scenario. Thus, off-transect ocean bottom pressure could provide additional information for reconstructing ocean transport.

Off-transect ocean bottom pressure is not directly physically linked to ocean transport in the same way that on-transect ocean bottom pressure is, without assuming that AABW transport is invariant with latitude. In order to include off-transect ocean bottom pressure in our reconstruction, we assume that AABW transport anomalies can be reconstructed from a weighted sum of ocean bottom pressure anomalies at different locations, where these weights can be positive or negative, and arbitrarily large:

$$\hat{\psi}_t = \sum_i w_i p_{i,t}, \tag{2}$$

where $\hat{\psi}_t$ is the predicted AABW transport at time t, w is the weight for a particular gridcell i, and p is the pressure for a gridcell i and time t. Note that i could cover any cell in the region of interest, and is not limited to a single dimension. This formulation is consistent with the linear relationship from physical theory in a one dimensional example, while also generalising to allow the incorporation of two dimensional ocean bottom pressure.

We use a least-squares linear regression with ridge regularisation to estimate weights for ocean bottom pressure: regularisation reduces overfitting to the training data by favour-

ing solutions with smaller weights, where noise contributes less to the final reconstruction (see, for example, McDonald (2009)). We fit the linear regression on 230 years of ACCESS-OM2-01 repeat year forced data, at monthly resolution, with the climatology removed. This data has, in effect, constant atmospheric forcing and thus the linear regression captures the ocean bottom pressure signal of unforced internal variability of AABW transport.

2.4 Processing of model output ocean bottom pressure

Ocean bottom pressure is output by the ACCESS-OM2-01 model. However, the output from ACCESS-OM2-01 is at 0.1° resolution, and estimating weights at this resolution numerically destabilises the linear regression, resulting in noisy weights and poor AABW transport reconstruction. To stabilise our weight calculation, we initially average ocean bottom pressure to 1° resolution. One degree resolution has been used by previous studies to evaluate the links between ocean transport and ocean bottom pressure (e.g. Solodoch et al., 2023).

We aim to not only probe the link between ocean bottom pressure and AABW transport, but also to apply our calculated weights to satellite observations of ocean bottom pressure and thereby estimate AABW transport. For this purpose, the ocean bottom pressure grid for which we calculate weights must align with an observational grid. The GRACE satellites observe temporal variations in ocean bottom pressure with a spatial resolution of around 300km (3° at the equator), and temporal resolution of 1 month. We use GRACE observations on a mascon (**mas**s **con**centration) grid, where anomalous mass is estimated as discrete homogeneous tiles of equivalent water height. These GRACE observations show improved separation of the relevant ocean signals from land signals, compared to previous GRACE observations estimated as spherical harmonic coefficients (Watkins et al., 2015). We base our AABW transport reconstruction on Jet Propulsion Laboratory (JPL) GRACE mascon product RL06.1Mv03 (Watkins et al., 2015). We find this product to have the lowest uncertainty of available GRACE mascon products when empirically validated against *in-situ* ocean bottom pressure (Section 2.5, Figure S2), though in some cases the difference is negligible.

To convert ACCESS-OM2-01 model output ocean bottom pressure to the same grid as satellite observations, we average the ACCESS-OM2-01 ocean bottom pressure to the

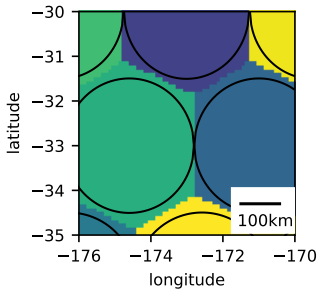

Figure 1. An example part of the JPL RL06.1Mv03 GRACE mascon grid. Black outlines represent the circular mascons that compose the grid. Colours indicate which mascon/gridpoint an ACCESS-OM2-01 gridcell is assigned to.

irregular ∼300km grid used by the JPL RL06.1Mv03 GRACE mascon product (Figure 1). This allows us firstly to estimate the impact of resolution in the model, and furthermore to calculate weights for ocean bottom pressure on this grid, which we can then transfer to satellite observations of ocean bottom pressure. This mascon grid is nominally composed of circles, which do not entirely cover the surface of the Earth. Nonetheless, ocean bottom pressure from the gaps between the circular mascons influences the calculated ocean bottom pressure in the mascons (Watkins et al., 2015), and so we average all ocean bottom pressure in the model onto the nearest circular mascon (Figure 1).

We omit ocean bottom pressure at some locations, due to unresolved uncertainty or signal contamination. The signals that the GRACE satellites measure on ice-free land – mostly changes in soil moisture and groundwater – have greater magnitude than the ocean bottom pressure signals. To prevent these land signals from contaminating our AABW transport estimate, we discard any mascon with more than 1% land as a fraction of total area. Glacial isostatic adjustment (GIA) is a substantial part of the mass change signal measured by the GRACE satellites (Caron et al., 2018). As this adjustment results from movement of mantle mass rather than ocean mass, it does not contribute to ocean bottom pressure. We use the default ICE6G-D model to correct for GIA (Peltier et al., 2018). Error from this GIA model will contribute to error in our calculated AABW trends. Our reconstructions only use mascons at a latitude north of ∼50° S, which should minimise this error (see Figure 3). We omit the impact of GIA in our error estimation, because this error is poorly characterised.

2.5 Uncertainty in satellite-based bottom pressure estimates

Measurement uncertainty in ocean bottom pressure leads to uncertainty in the reconstruction of AABW. We estimate the uncertainty of GRACE satellite observations of ocean bottom pressure by empirically comparing GRACE observations to *in-situ* ocean bottom pressure records from the Permanent Service for Mean Sea Level database (Permanent Service for Mean Sea Level, 2022). We limit *in-situ* ocean bottom pressure records to those with a length of at least 12 months and no gaps greater than a month: a total of 1798 months of data from 88 ocean bottom pressure sensor deployments meet this criteria. All deployments included in this database are from earlier than 2016. We average the *in-situ* records to the same monthly epochs as GRACE and compare each *in-situ* deployment to the GRACE mascon covering its location (Figure 2a). We do not find any systematic link between GRACE error and any of latitude, ocean basin or ocean depth, and therefore combine the error from all ocean bottom pressure sensor deployments. We iteratively estimate a standard deviation, discarding outliers more than three standard deviations from the mean until the estimate converges (difference in subsequent error estimates is less than 10^{-3} dbar). Using this method, we estimate that the root mean square error (RMSE) of JPL GRACE solutions is 0.015 dbar (Figure 2b). This error is added to the AABW transport reconstruction error by Gaussian error propagation (Lo, 2005), adjusting the sum of squared error to be:

$$\sum_t (\psi_t - \hat{\psi}_t)^2 + \sum_t \sum_i \sigma^2 w_i^2, \tag{3}$$

where σ represents the RMSE of GRACE observations. In applying this formula, we assume that GRACE error is neither spatially nor temporally correlated. (Note that this assumption is not strictly true: error in temporally adjacent mascon estimates has a weak correlation of r$\sim$0.3, and error in spatially adjacent mascons is known to be correlated, but is difficult to quantify.)

Ocean bottom pressure sensors, which we use as ground-truth, are known to drift with greater magnitude than ocean variability (Polster et al., 2009). This drift is best removed with an empirical exponential plus linear trend (Polster et al., 2009), and is already removed from the bottom pressure records we use. We elect not to detrend the GRACE observations, because this would remove one degree of freedom from already short timeseries (mean length of 20 months per *in-situ* record). This choice could lead

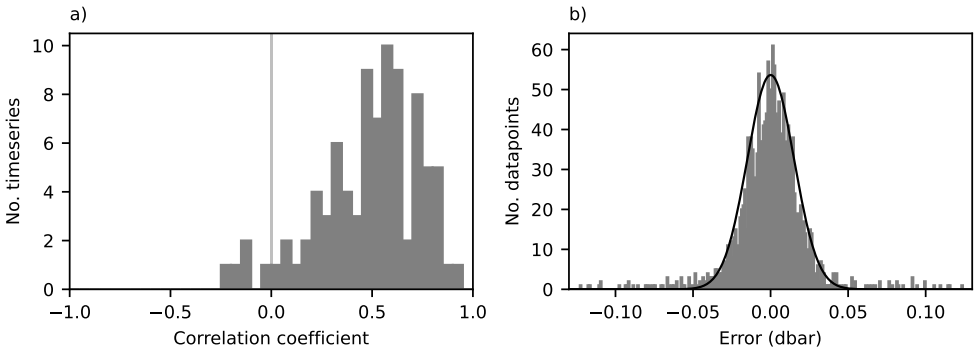

Figure 2. Empirical validation of JPL GRACE observations using *in-situ* ocean bottom pressure records. a) Histogram of Pearson's correlation coefficient between each deployment and the corresponding GRACE estimate of ocean bottom pressure. Bin width is 0.05. b) Histogram of GRACE error relative to *in-situ* ocean bottom pressure observations combined from all *in-situ* records. Bin width is 0.001. Black line shows estimated Gaussian error with a RMSE of 0.015 dbar.

to overestimating the error, but detrending the GRACE observations decreases error by less than 10%.

We also assume that any difference between the *in-situ* measurement and the GRACE observation is exclusively due to GRACE measurement error. Additional deviation related to the comparison of point measurements to 300km averages, or from error in the *in-situ* records, would result in some overestimation of GRACE error. A comparison of high resolution and spatially coarsened ocean bottom pressure anomalies in ACCESS-OM2-01 suggests that averaging imparts some error, possibly reducing the raw error by 30%, but this error is uncorrelated with the total error of any given *in-situ* record and we do not attempt to remove it. This choice means that our uncertainty estimate is more conservative than estimates used in previous work (e.g Mazloff & Boening, 2016).

2.6 Reconstruction optimisation

To optimise our reconstruction method, we use the coefficient of determination (R^2) between the validation and reconstructed AABW transport timeseries as a metric of skill. There are, confusingly, multiple skill metrics termed R^2 (Kvalseth, 1985). Here, we cal-

culate:

$$\mathrm{R}^2 = 1 - \frac{\sum_t (\psi_t - \hat{\psi}_t)^2}{\sum_t (\psi_t - \bar{\psi}_t)^2}, \tag{4}$$

where an overbar ($^-$) indicates a time-mean. This measure of skill is not generally equivalent to the square of Pearson's correlation coefficient (r^2) (Kvalseth, 1985). Addition of noise from measurement error adjusts R^2 to:

$$\mathrm{R}^2 = 1 - \frac{\sum_t (\psi_t - \hat{\psi}_t)^2 + \sum_t \sum_i \sigma^2 w_i^2}{\sum_t (\psi_t - \bar{\psi}_t)^2}, \tag{5}$$

The reconstruction method is primarily optimised in an empirical fashion. For each component of the reconstruction method (e.g. data used, temporal smoothing, etc), we test a range of values and select those which maximise the reconstruction skill in the historically forced run of ACCESS-OM2-01. The strength of ridge regularisation is empirically determined for each transect independently – stronger regularisation is required for the reconstructions where noise makes up a greater part of the input data. Other optimal architecture choices are used consistently across reconstructions, and are listed as follows:

- The latitudinal range of ocean bottom pressure information is $\pm 10°$ of the transect.
- The ocean bottom pressure and AABW transport are smoothed with a Gaussian filter with standard deviation of four months, after removing the seasonal cycle.
- Instead of fitting a single linear regression to each basin, we fit a regression to calculate the weights for each AABW pathway through a basin and later combine these to full basin transports. For example, we split the Atlantic into two sub-basins on each side of the mid-ocean ridge. The subbasins are defined following AABW pathways in Figure 4 of Solodoch et al. (2022).

The reasoning for the first two optimisation choices producing highest skill is unclear; they were simply empirically chosen after evaluating a range of values (Figures S3, S4). We propose that the third may improve skill by decreasing the number of weights to be fitted for the same length of training data. The transects across which AABW transport is reconstructed and the ocean bottom pressure range used for this reconstruction is represented visually in Figure 3.

Historical changes in ocean bottom pressure are dominated by ocean mass increase from melting ice sheets and glaciers. Ocean mass gain produces an ocean bottom pres-

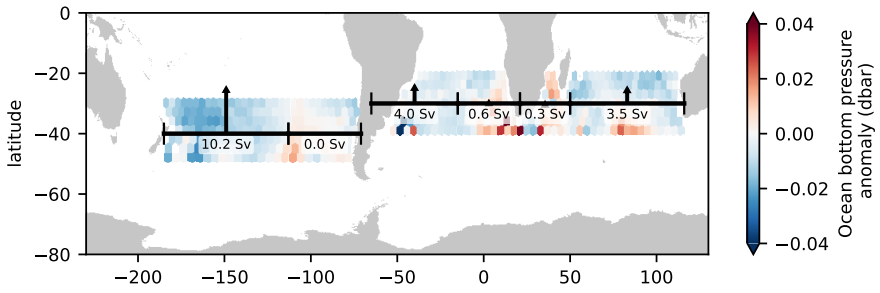

Figure 3. A schematic of the data used for AABW transport reconstruction from ocean bottom pressure. In each ocean basin, the transects across which AABW transport is calculated are marked in black, as is the mean AABW transport across each of these transects. Colors show ocean bottom pressure from a single timestep in ACCESS-OM2-01 averaged onto the JPL mascon grid, and trimmed to the latitude ranges used to reconstruct AABW.

sure signal of around 0.02 dbar per decade (Johnson & Chambers, 2013); ocean bottom pressure variations related to interannual variability in ocean transport are around 0.02 dbar (Landerer et al., 2015). However, this long-term trend in ocean bottom pressure is not incorporated into the ocean model simulations. The linear regression weights need to be robust to ocean mass gain, otherwise mass gain will produce a spurious trend in the final AABW transport estimate. To ensure this robustness, we duplicate the training data for the linear regression and add a basin-wide 1 dbar to ocean bottom pressure in the second half of this training data, but leave the AABW transport unmodified. We hereby fit a linear regression to a timeseries which is twice as long, and the same ocean transport occurs twice in the timeseries, the second time with a basin-wide 1 dbar increase in ocean bottom pressure. The linear regression is therefore forced to ignore basin-wide ocean mass changes. We show that this method is effective at removing all dependency on basin-wide sea level by adding a 0.5 dbar gradual increase to ocean bottom pressure and observing the impact (Figure 4).

3 Evaluation of method

This section presents our method's skill at reconstructing AABW transport from ocean bottom pressure. We initially illustrate the physical mechanism behind reconstruction skill with one example transect. We then quantify reconstruction skill across all basins, and explore the impact of realistic bottom pressure measurement constraints – resolu-

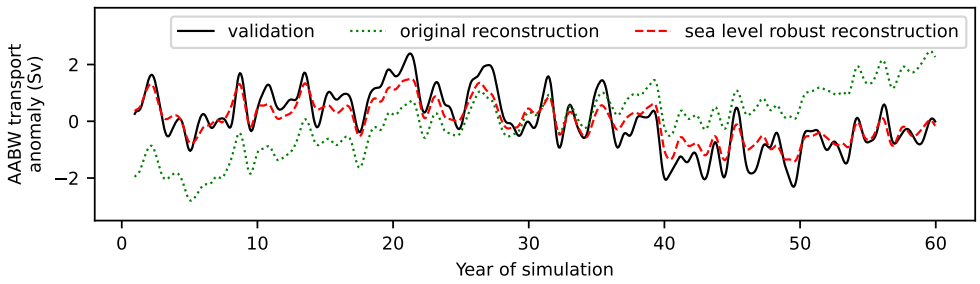

Figure 4. Reconstructions with and without accounting for basin-wide ocean mass gain. The black line shows AABW in ACCESS-OM2-01 validation data. Both reconstructions use the same model ocean bottom pressure output with a trend of 0.5 dbar increase over the full time period. This trend affects the original non-robust linear regression (green dotted line), but not the one which is trained to be robust against basin-wide sea level changes (red dashed line).

tion and noise – on reconstruction skill. Finally, we test our reconstruction method on output from independent ocean models, to more robustly estimate reconstruction skill, including the impact of model biases. These estimates of skill are interpreted to inform future improvements in reconstruction.

3.1 Detailed examination of one specific reconstruction

To demonstrate the physical reasoning behind our AABW transport reconstruction method, we initially examine the method in one sector of the Southern Ocean. For this purpose we reconstruct AABW transport in the western Pacific, from model output ocean bottom pressure averaged onto a 1° grid. To reconstruct AABW, our method uses a linear regression to estimate a set of weights by which to multiply ocean bottom pressure (Section 2). The distribution of these weights can be displayed spatially, to indicate the patterns of ocean bottom pressure which the linear regression associates with AABW transport: Figure 5a shows the weights used to reconstruct AABW transport in the western Pacific. Positive weights are found on the western boundary below 3000 m, approximately the depth of the AABW layer in ACCESS-OM2-01. Conversely, negative weights are found towards the mid-ocean ridge on the eastern side of the sub-basin. This distribution of weights relates a decrease in pressure with increasing longitude to northward AABW transport, in agreement with physical theory derived from geostrophic flow (Hughes et al., 2013).

In addition to aligning with physical theory, the weights we calculate can be effective at reconstructing AABW transport. The weights were derived from ACCESS-OM2-01 repeat year forced model output. We test these weights on the historically forced ACCESS-OM2-01 run, and generate a reconstruction from this independent ocean bottom pressure. The reconstruction (black line in Figure 5c) accounts for 88% of AABW transport variance in the historically forced run (grey line in Figure 5c). Thus, our reconstruction method can produce skilful reconstructions of AABW transport, at least when using ocean bottom pressure at 1° resolution.

A more realistic demonstration of our reconstruction method would incorporate the constraints imposed by satellite-observed ocean bottom pressure. These constraints include two factors: the ∼300 km spatial resolution of existing satellite ocean bottom pressure observations, and their measurement uncertainty. We calculate weights for ocean bottom pressure averaged onto a grid used operationally for satellite ocean bottom pressure estimates (see Figures 1 and 3), and with the linear regression regularisation tuned to mitigate the effects of observational ocean bottom pressure uncertainty (standard deviation 0.015 dbar; see methods and Figure 2). These new weights (Figure 5b) are consistent with the weights in Figure 5a, albeit at lower resolution. Therefore, the lower resolution weights still agree with physical theory (Hughes et al., 2013). The coarser resolution of ocean bottom pressure results in a wider band of positive weights on the western boundary, which Hughes et al. (2018) argued limit the effectiveness of GRACE satellite observations. The decrease in resolution, combined with the addition of noise, reduces reconstruction skill to capture 75% of AABW transport variance (see dashed line in Figure 5c).

3.2 Quantifying AABW reconstruction skill

We now expand our analysis to encompass all three ocean basins, and to further test how skill is impacted by the resolution and uncertainty of satellite-measured ocean bottom pressure. We perform this analysis using two skill metrics: coefficient of determination (R^2) and mean square error. R^2 shows relative skill as a percentage of variance captured. Mean squared error, though less intuitive than root mean squared error, has the advantage that independent Gaussian sources of error sum linearly. Higher R^2 and lower mean squared error each indicate greater skill. These skill metrics are evaluated

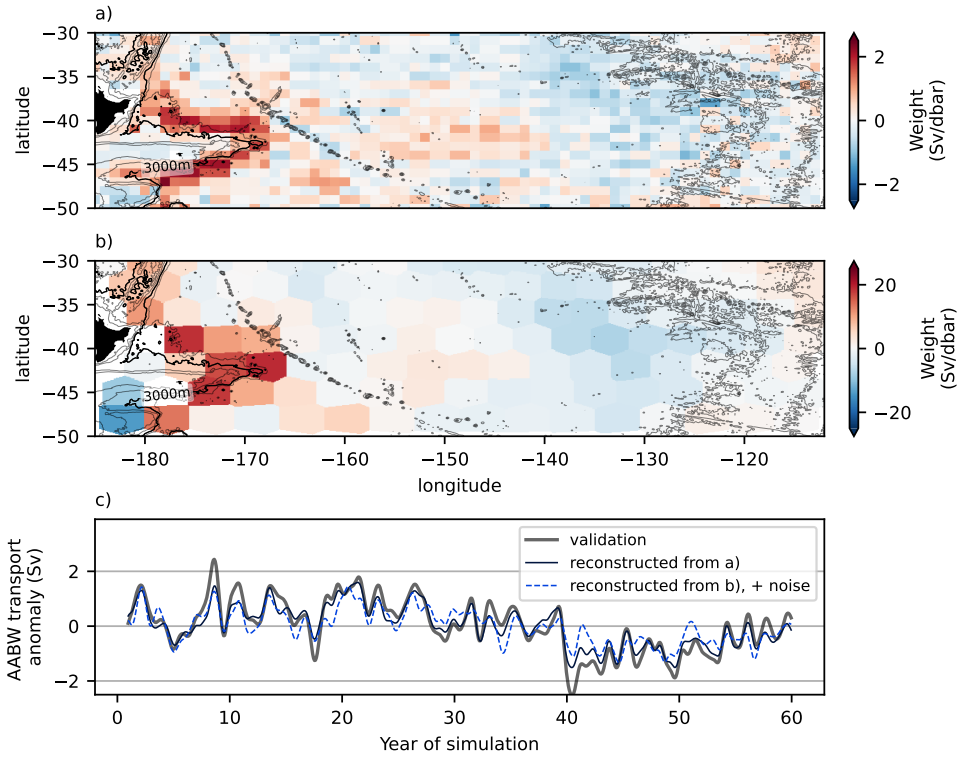

Figure 5. AABW transport anomaly reconstruction at 40°S in the west Pacific Ocean from ACCESS-OM2-01 repeat year forced model output ocean bottom pressure. a) Spatial pattern of weights from the linear regression of ocean bottom pressure coarsened to 1° resolution upon AABW transport. b) Spatial pattern of weights from the linear regression for ocean bottom pressure which is coarsened onto the ∼300km grid used in JPL GRACE processing. c) Validation AABW transport, along with reconstructions from the weights in a) and b). These weights reconstruct validation AABW transport with reasonable skill: R^2 is 0.88 and 0.75 respectively. The reconstruction from ocean bottom pressure coarsened to ∼300km has noise added to mimic the uncertainty of GRACE satellite observations of ocean bottom pressure.

in Figure 6 as a function of ocean bottom pressure resolution and additional noise, in each ocean basin.

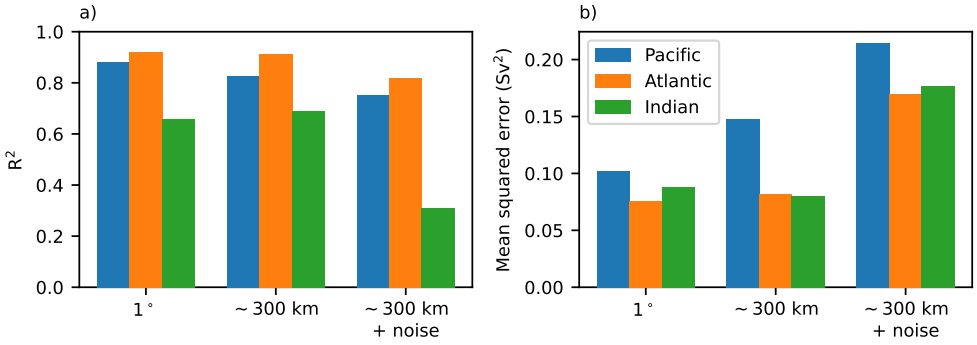

Figure 6. Skill of AABW reconstructions from each of ocean bottom pressure coarsened to 1 degree resolution (left bars), averaged onto JPL mascon shapes (approximately 3° resolution; centre bars), and averaged onto the JPL mascon shapes with noise added (right bars). a) shows the coefficient of determination, or R^2, which quantifies the fraction of variance captured by the reconstruction. b) shows mean square error which quantifies the absolute error of the reconstruction, against a total variance of 0.85, 0.92 and 0.26 Sv^2 for the Pacific, Atlantic and Indian Oceans respectively.

We start with ocean bottom pressure coarsened to 1° resolution, because this reconstruction is not coarsened beyond what is needed numerically and is not inhibited by noisy ocean bottom pressure. Therefore, any error indicates limitations of the reconstruction method itself. This reconstruction, using ocean bottom pressure at 1° resolution with no noise, captures 65-90% of AABW transport variance, depending on the ocean basin (Figure 6a, left bars). Reconstructions are generally most skilful in the Atlantic Ocean, and least skilful in the Indian Ocean. Variation between basins is dependent on the isopycnal used to define AABW (not shown) and the latitude at which AABW transport is calculated (Figure S5). These two changes would impact AABW variance or transect bathymetry, as would changing ocean basins, so we suggest that AABW variance or transect bathymetry contribute to changes in reconstruction skill. Our reconstruction skill is similar to the reconstructions from Solodoch et al. (2023) that use a linear regression with regularisation and we conclude that our method is a viable approach to reconstruct AABW transport from precise, high resolution measurements of ocean bottom pressure.

To test the impact of ocean bottom pressure resolution on reconstruction skill, we compare reconstructions from ocean bottom pressure coarsened to 1° and ∼300 km. The percentage of variance captured (R^2) by reconstructions using the two different resolutions of ocean bottom pressure are within 6% (compare left and centre groups of bars in Figure 6a). Changes in mean squared error are generally small, with the exception that mean squared error in the Pacific Ocean increases by 45% (Figure 6b). This increase suggests that the lower resolution ocean bottom pressure doesn't resolve some relevant feature of ocean bottom pressure anomalies in the Pacific Ocean. In the Indian Ocean, the lower resolution ocean bottom pressure (∼300 km) produces slightly (ΔR^2 ≈5%) better reconstructions of AABW transport than the high resolution ocean bottom pressure (1°). We hypothesise that having fewer weights numerically stabilises the linear regression or reduces overfitting, resulting in a minor increase in skill. In summary, ocean bottom pressure resolution has some, mostly small, impact on reconstruction skill, consistent with previous skilful reconstructions from ocean bottom pressure at ∼300km resolution (Bentel et al., 2015; Landerer et al., 2015). In contrast to the suggestion of Hughes et al. (2018), we find that ocean bottom pressure at lower resolution can be used to effectively estimate AABW transport.

To test the impact of uncertainty on the reconstruction, we emulate the uncertainty of satellite ocean bottom pressure measurements with added noise. The inclusion of realistic uncertainty increases the mean squared error by up to a factor of 2 (compare centre and right groups of bars in Figure 6b), and lowers the R^2 by 10-35% (compare centre and right groups of bars in Figure 6a). We find that this uncertainty reduces reconstruction skill far more than the low spatial resolution does, in all three ocean basins.

3.3 Evaluation using other ocean models

We further evaluate our reconstruction method with data from two additional ocean models. Any empirical model, including our reconstruction method and weights, is dependent on the system upon which it is trained being representative of the real world. Because we train and test our reconstruction method in ACCESS-OM2-01, any biases or misrepresentations in ACCESS-OM2-01 are likely to also exist in our reconstruction method. A simple way to test the magnitude of error from these biases is to evaluate the method using output from a different ocean model, which we expect to have different biases. We use both ACCESS-OM2-025, the same model as our training data but at a

different resolution, and GFDL-OM4-025, which has different ocean and sea ice components. We apply the weights calculated from ACCESS-OM2-01 to bottom pressure from the other models, and compare the resultant reconstruction to the AABW from these models (Figure 7). R^2 and MSE vary between reconstructions in different models and in different basins. The spread in reconstruction error leads to a range of possible uncertainties in our final AABW reconstruction. With the caveat that only two different numerical models are used to test generalisability here, we expect our error in reconstructions from GRACE observational data to be in the range of errors from validation in different models. To be conservative, we take the error from the model where reconstruction error is largest for our uncertainty estimate in Section 4. Part of the variation in error may be explained by changes in the variance of smoothed AABW transport (shown explicitly in Figure S6, and implicitly in the way R^2 changes in conjunction with MSE). Nonetheless, R^2 and MSE are of similar magnitude in all models. This result lends confidence to our method, and to our final reconstructions from GRACE observational data in Section 4.

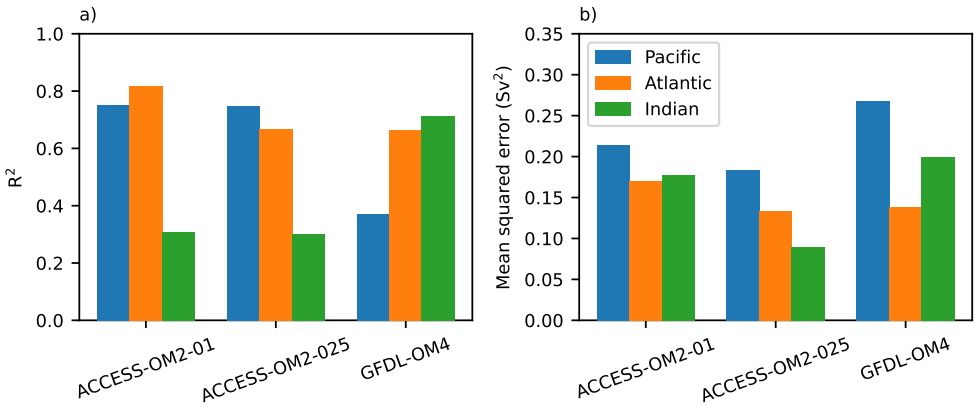

Figure 7. Skill of AABW transport reconstructions when evaluated in different ocean models: two ACCESS-OM2 runs at different resolution, both with historical forcing, and GFDL-OM4 with a repeat year forcing. a) shows the coefficient of determination, or R^2, which quantifies the fraction of variance captured by the reconstruction. b) shows mean square error, which quantifies the absolute error of the reconstruction. In all three test cases, the weights come from a fit to ACCESS-OM2-01, and use ocean bottom pressure coarsened to ∼300 km with added noise.

4 An AABW transport timeseries

We use our optimised reconstruction method, and observations from the GRACE satellites, to create a timeseries of AABW transport anomalies in each ocean basin (Figure 8). A two-sigma confidence interval is shaded, where the standard deviation is conservatively taken as the square root of the mean square error in the model with worst error (Figure 7b) for each basin. The error in the reconstruction is substantial, such that the two-sigma confidence intervals of the reconstructions (shown in red shading) almost always encompass the 0 Sv anomaly. Both the two-sigma interval and R^2 around 0.5 should be considered when interpreting these reconstructions: although the error in our reconstruction is substantial, we assume based on the models' R^2 metric of skill (Figure 7) that the fraction of ocean MOC variance that our reconstruction captures is around 50%.

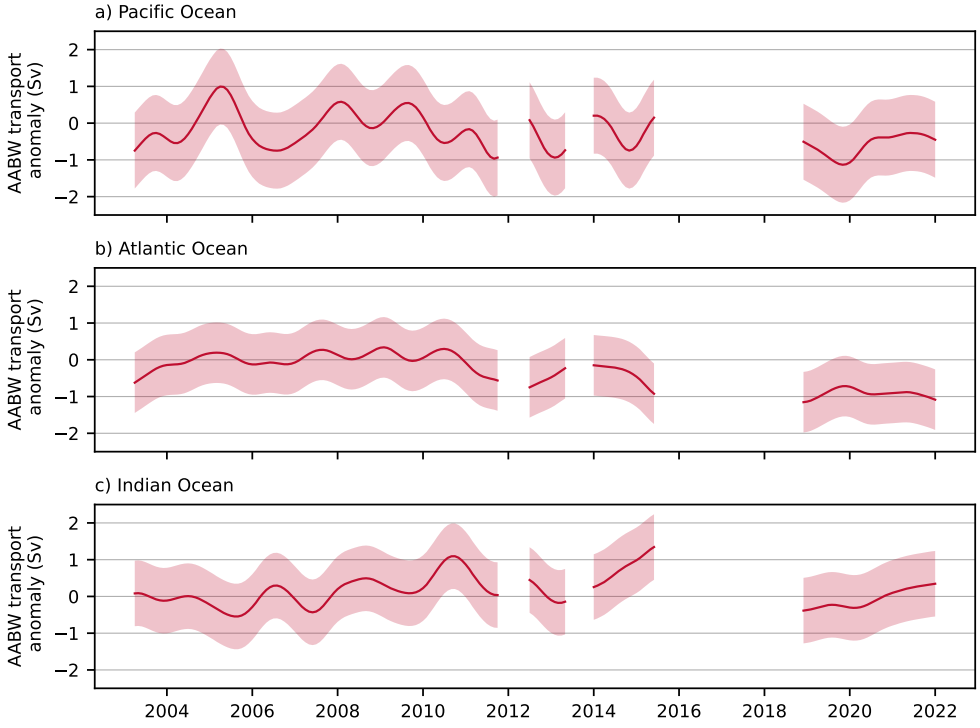

Figure 8. Reconstructed AABW transport anomaly from satellite observations of ocean bottom pressure. Gaps in data indicate times when no GRACE data is available – specifically when less than three quarters of the data needed for the temporally smoothed average is available. The data has been smoothed with a Gaussian filter with a standard deviation of four months. Errorbars show the two-sigma range – approximately the 95% confidence interval – and include both observational and methodological uncertainty.

We can also calculate a trend of our AABW transport reconstruction, from the unsmoothed timeseries (Table 2). These trends are, for the most part, not significantly different from zero, because the estimated error is large. Therefore, they are more useful for establishing an upper bound on changes than to actually quantify trends. We do find a trend in Atlantic AABW transport outside our quoted uncertainty. However, trends in GRACE satellite observations of ocean bottom pressure are impacted by the choice of GIA model (Caron et al., 2018), used to correct the GRACE observations for solid Earth changes. The GIA uncertainty is not included in our uncertainty estimate. As such, our presented trends may be subject to higher error than quoted.

Our estimates of AABW transport trends are consistent with previous estimates. Kouketsu et al. (2011) found trends in AABW volume of -0.71, -0.43 and 0.17 Sv/decade changes in AABW transport at 35°S in the Pacific, Atlantic and Indian Oceans respectively. These trends are within the uncertainty of our AABW transport trends in the Atlantic and Indian Oceans, and of similar magnitude to our uncertainty estimate in the Pacific. Consistent with our results in the Atlantic Ocean, Johnson (2022) found a loss of 0.9 Sv of geostrophic AABW transport in the Argentine basin over a period of 20-40 years. The epochs used to calculate trends could impact the trend, given the internal variability in AABW transport (Figure 8). The uncertainty in our estimates of AABW transport trends encompasses both previous trend estimates and no trend, and so we do not provide new information on this particular question. Given our error, we would be able to observe a change of $\sim$1 Sv (after the low-pass filter we employ), which would mean the projected AABW response to climate change in Li et al. (2023) would be measurable in the 2040s.

Table 2. Trends in AABW transport, reconstructed from GRACE satellite observations of ocean bottom pressure. Uncertainty indicates a 2σ value.

Ocean	Trend
Pacific	-0.08±0.35 Sv/decade
Atlantic	-0.55±0.20 Sv/decade
Indian	0.05±0.20 Sv/decade

5 Conclusions

We explore how best to use observations of ocean bottom pressure from the GRACE satellites as a proxy to reconstruct AABW, using a linear regression framework. We estimate sources of error in these reconstructions by quantifying reconstruction skill in scenarios of increasing realism, starting with a simple reconstruction of ocean model AABW transport from ocean model bottom pressure, and sequentially including error from resolution, measurement uncertainty and ocean model biases. At the end of this process, we use our reconstruction method and our combined uncertainty estimate to present a timeseries of AABW transport from satellite observations of ocean bottom pressure.

The sensitivity of the framework to the quality of ocean bottom pressure data highlights several important aspects of this method. First, ocean bottom pressure with lower spatial resolution does not unduly affect the output. Conversely, additional noise inserted to mimic satellite observation quality degrades the reconstruction skill of AABW transport. The reconstruction skill in each of the three ocean basins responds similarly to changes in the structure of ocean bottom pressure data: in each case the resolution of ocean bottom pressure has minimal impact on skill, while the addition of noise consistently decreases skill. Finally, we show that the reconstruction method broadly generalises to other ocean models – error is the same order of magnitude – but the variability suggests that evaluation in additional models or improved dynamical understanding of variations in error could improve error estimates.

AABW transport reconstructions could be most improved by addressing ocean bottom pressure measurement uncertainty, as we find that the addition of measurement-like noise causes the largest reduction in simulated reconstruction skill. Newer releases of GRACE products are generally more accurate than older releases, and thus future improvements in the accuracy of GRACE satellite observations are likely (Macrander et al., 2010; Chambers & Bonin, 2012). Mass change is a designated observable by the National Aeronautics and Space Administration (NASA), and there are plans for future mass change satellite missions (Wiese et al., 2022). More accurate ocean bottom pressure observations could be used for improved estimates of ocean transport. Given the large impact of adding noise to the ocean bottom pressure, future work investigating ocean transport reconstruction from ocean bottom pressure should incorporate the uncertainty of GRACE observations.

We further suggest including additional observables to improve the accuracy of AABW transport reconstructions. Some error remains in reconstructions from 1° noise-free ocean bottom pressure, suggesting that alternate sources of data or reconstruction methods may improve AABW transport reconstructions. Stewart et al. (2021) suggest that zonal wind stress would be skilful at reconstructing AABW transport, and Solodoch et al. (2023) find that combining zonal wind stress with ocean bottom pressure offers slight improvements in reconstructions over using solely ocean bottom pressure. Given the reduction in accuracy from GRACE noise, further exploration of including wind stress measurements is justified. *In-situ* observations, such as data from more recent deep Argo data or mooring arrays, could be combined with our estimate to constrain AABW interannual variations.

This work provides a first estimate of interannual AABW transport variability from the currently available GRACE satellite data. Variations in AABW transport of magnitude >1 Sv over several years (around 1-10% of total AABW transport) would be detectable with our method. Additionally, we demonstrate a method of using satellite-measured ocean bottom pressure to infer AABW transport anomalies, and a method of including the impacts of both satellite resolution and measurement uncertainty in our error estimate. Satellite measurement uncertainty is the largest contributor to uncertainty in our AABW transport reconstruction: future work to refine estimates of AABW transport from satellite observations of ocean bottom pressure will need to develop methods to minimise the impact of measurement uncertainty.

6 Open Research

Code used to perform the analyses and processed model output will be uploaded to zenodo once the manuscript is accepted. (Code is currently here: https://github.com/jemmajeffree/grace-aabw)

The JPL GRACE/GRACE-FO Mascon data are available at http://grace.jpl.nasa.gov

In situ ocean bottom pressure records are available at https://www.psmsl.org/data/bottom_pressure/

References

Abrahamsen, E. P., Meijers, A. J. S., Polzin, K. L., Naveira Garabato, A. C., King, B. A., Firing, Y. L., ... Meredith, M. P. (2019). Stabilization of dense Antarc-

tic water supply to the Atlantic Ocean overturning circulation. *Nature Climate Change*, *9*(10), 742–746. Retrieved from https://doi.org/10.1038/s41558-019-0561-2 doi: 10.1038/s41558-019-0561-2

Adcroft, A., Anderson, W., Balaji, V., Blanton, C., Bushuk, M., Dufour, C. O., ... Zhang, R. (2019). The GFDL global ocean and sea ice model OM4.0: Model description and simulation features. *Journal of Advances in Modeling Earth Systems*, *11*(10), 3167-3211. Retrieved from https://agupubs.onlinelibrary.wiley.com/doi/abs/10.1029/2019MS001726 doi: https://doi.org/10.1029/2019MS001726

Bentel, K., Landerer, F. W., & Boening, C. (2015). Monitoring Atlantic overturning circulation and transport variability with GRACE-type ocean bottom pressure observations – a sensitivity study. *Ocean Science*, *11*(6), 953–963. Retrieved from https://os.copernicus.org/articles/11/953/2015/ doi: 10.5194/os-11-953-2015

Bingham, R. J., & Hughes, C. W. (2008). Determining North Atlantic meridional transport variability from pressure on the western boundary: A model investigation. *Journal of Geophysical Research: Oceans*, *113*(C9). Retrieved from https://agupubs.onlinelibrary.wiley.com/doi/abs/10.1029/2007JC004679 doi: https://doi.org/10.1029/2007JC004679

Caron, L., Ivins, E. R., Larour, E., Adhikari, S., Nilsson, J., & Blewitt, G. (2018). GIA model statistics for GRACE hydrology, cryosphere, and ocean science. *Geophysical Research Letters*, *45*(5), 2203-2212. Retrieved from https://agupubs.onlinelibrary.wiley.com/doi/abs/10.1002/2017GL076644 doi: https://doi.org/10.1002/2017GL076644

Chambers, D. P., & Bonin, J. A. (2012). Evaluation of release-05 GRACE time-variable gravity coefficients over the ocean. *Ocean Science*, *8*(5), 859–868. Retrieved from https://os.copernicus.org/articles/8/859/2012/ doi: 10.5194/os-8-859-2012

Foppert, A., Rintoul, S. R., Purkey, S. G., Zilberman, N., Kobayashi, T., Sallèe, J.-B., ... Wallace, L. O. (2021). Deep Argo reveals bottom water properties and pathways in the Australian-Antarctic basin. *Journal of Geophysical Research: Oceans*, *126*(12), e2021JC017935. Retrieved from https://agupubs.onlinelibrary.wiley.com/doi/abs/10.1029/2021JC017935

(e2021JC017935 2021JC017935) doi: https://doi.org/10.1029/2021JC017935

Fukamachi, Y., Rintoul, S. R., Church, J. A., Aoki, S., Sokolov, S., Rosenberg, M. A., & Wakatsuchi, M. (2010, 4). Strong export of Antarctic Bottom Water east of the Kerguelen plateau. *Nature Geoscience*, *3*(5), 327–331. Retrieved from http://dx.doi.org/10.1038/NGEO842 doi: 10.1038/ngeo842

Hughes, C. W., Elipot, S., Maqueda, M. Á. M., & Loder, J. W. (2013). Test of a method for monitoring the geostrophic Meridional Overturning Circulation using only boundary measurements. *Journal of Atmospheric and Oceanic Technology*, *30*(4), 789 - 809. Retrieved from https://journals.ametsoc.org/view/journals/atot/30/4/jtech-d-12-00149_1.xml doi: 10.1175/JTECH-D-12-00149.1

Hughes, C. W., Williams, J., Blaker, A., Coward, A., & Stepanov, V. (2018). A window on the deep ocean: The special value of ocean bottom pressure for monitoring the large-scale, deep-ocean circulation. *Progress in Oceanography*, *161*, 19-46. Retrieved from https://www.sciencedirect.com/science/article/pii/S0079661117303154 doi: https://doi.org/10.1016/j.pocean.2018.01.011

Ivchenko, V. O., Sidorenko, D., Danilov, S., Losch, M., & Schröter, J. (2011). Can sea surface height be used to estimate oceanic transport variability? *Geophysical Research Letters*, *38*(11). Retrieved from https://agupubs.onlinelibrary.wiley.com/doi/abs/10.1029/2011GL047387 doi: https://doi.org/10.1029/2011GL047387

Johnson, G. C. (2008). Quantifying Antarctic Bottom Water and North Atlantic Deep Water volumes. *Journal of Geophysical Research: Oceans*, *113*(C5). Retrieved from https://agupubs.onlinelibrary.wiley.com/doi/abs/10.1029/2007JC004477 doi: https://doi.org/10.1029/2007JC004477

Johnson, G. C. (2022). Antarctic Bottom Water warming and circulation slowdown in the Argentine Basin from analyses of deep Argo and historical shipboard temperature data. *Geophysical Research Letters*, *49*(18), e2022GL100526. Retrieved from https://agupubs.onlinelibrary.wiley.com/doi/abs/10.1029/2022GL100526 (e2022GL100526 2022GL100526) doi: https://doi.org/10.1029/2022GL100526

Johnson, G. C., & Chambers, D. P. (2013). Ocean bottom pressure seasonal cycles and decadal trends from GRACE release-05: Ocean circulation implications.

Journal of Geophysical Research: Oceans, *118*(9), 4228-4240. Retrieved from https://agupubs.onlinelibrary.wiley.com/doi/abs/10.1002/jgrc.20307 doi: https://doi.org/10.1002/jgrc.20307

Kiss, A. E., Hogg, A. M., Hannah, N., Boeira Dias, F., Brassington, G. B., Chamberlain, M. A., ... Zhang, X. (2020). ACCESS-OM2 v1.0: a global ocean–sea ice model at three resolutions. *Geoscientific Model Development*, *13*(2), 401–442. Retrieved from https://gmd.copernicus.org/articles/13/401/2020/ doi: 10.5194/gmd-13-401-2020

Kosempa, M., & Chambers, D. P. (2014, 2022/01/31). Southern Ocean velocity and geostrophic transport fields estimated by combining Jason altimetry and Argo data [https://doi.org/10.1002/2014JC009853]. *Journal of Geophysical Research: Oceans*, *119*(8), 4761–4776. Retrieved from https://doi.org/10.1002/2014JC009853 doi: https://doi.org/10.1002/2014JC009853

Kouketsu, S., Doi, T., Kawano, T., Masuda, S., Sugiura, N., Sasaki, Y., ... Awaji, T. (2011). Deep ocean heat content changes estimated from observation and reanalysis product and their influence on sea level change. *Journal of Geophysical Research: Oceans*, *116*(C3). Retrieved from https://agupubs.onlinelibrary.wiley.com/doi/abs/10.1029/2010JC006464 doi: https://doi.org/10.1029/2010JC006464

Kvalseth, T. O. (1985, 2023/09/26/). Cautionary note about R^2. *The American Statistician*, *39*(4), 279–285. Retrieved from http://www.jstor.org/stable/2683704 doi: 10.2307/2683704

Landerer, F. W., Wiese, D. N., Bentel, K., Boening, C., & Watkins, M. M. (2015). North Atlantic Meridional Overturning Circulation variations from GRACE ocean bottom pressure anomalies. *Geophysical Research Letters*, *42*(19), 8114-8121. Retrieved from https://agupubs.onlinelibrary.wiley.com/doi/abs/10.1002/2015GL065730 doi: https://doi.org/10.1002/2015GL065730

Li, Q., England, M. H., Hogg, A. M., Rintoul, S. R., & Morrison, A. K. (2023). Abyssal ocean overturning slowdown and warming driven by Antarctic meltwater. *Nature*, *615*(7954), 841–847. Retrieved from https://doi.org/10.1038/s41586-023-05762-w doi: 10.1038/s41586-023-05762-w

Lo, E. (2005). Gaussian error propagation applied to ecological data: post-ice-storm-downed woody biomass. *Ecological Monographs*, *75*(4), 451-466. Retrieved

683 from https://esajournals.onlinelibrary.wiley.com/doi/abs/10.1890/
684 05-0030 doi: https://doi.org/10.1890/05-0030

685 Lumpkin, R., & Speer, K. (2007). Global ocean meridional overturning. *Jour-*
686 *nal of Physical Oceanography*, *37*(10), 2550 - 2562. Retrieved from https://
687 journals.ametsoc.org/view/journals/phoc/37/10/jpo3130.1.xml doi: 10
688 .1175/JPO3130.1

689 Macrander, A., Böning, C., Boebel, O., & Schröter, J. (2010). Validation
690 of GRACE gravity fields by in-situ data of ocean bottom pressure. In
691 F. M. Flechtner et al. (Eds.), *System earth via geodetic-geophysical space*
692 *techniques* (pp. 169–185). Berlin, Heidelberg: Springer Berlin Heidelberg.
693 Retrieved from https://doi.org/10.1007/978-3-642-10228-8_14 doi:
694 10.1007/978-3-642-10228-8_14

695 Mazloff, M. R., & Boening, C. (2016). Rapid variability of Antarctic Bot-
696 tom Water transport into the Pacific Ocean inferred from GRACE
697 [https://doi.org/10.1002/2016GL068474]. *Geophysical Research Letters*, *43*(8),
698 3822–3829. Retrieved from https://doi.org/10.1002/2016GL068474 doi:
699 https://doi.org/10.1002/2016GL068474

700 McDonald, G. C. (2009). Ridge regression. *WIREs Computational Statistics*, *1*(1),
701 93-100. Retrieved from https://wires.onlinelibrary.wiley.com/doi/abs/
702 10.1002/wics.14 doi: https://doi.org/10.1002/wics.14

703 Peltier, W. R., Argus, D. F., & Drummond, R. (2018). Comment on "an assess-
704 ment of the ICE-6G_c (VM5a) Glacial Isostatic Adjustment Model" by Pur-
705 cell et al. *Journal of Geophysical Research: Solid Earth*, *123*(2), 2019-2028.
706 Retrieved from https://agupubs.onlinelibrary.wiley.com/doi/abs/
707 10.1002/2016JB013844 doi: https://doi.org/10.1002/2016JB013844

708 Permanent Service for Mean Sea Level. (2022). *Ocean bottom pressure records.* Re-
709 trieved from https://www.psmsl.org/data/bottom_pressure/

710 Polster, A., Fabian, M., & Villinger, H. (2009). Effective resolution and drift of paro-
711 scientific pressure sensors derived from long-term seafloor measurements. *Geo-*
712 *chemistry, Geophysics, Geosystems*, *10*(8). Retrieved from https://agupubs
713 .onlinelibrary.wiley.com/doi/abs/10.1029/2009GC002532 doi: https://
714 doi.org/10.1029/2009GC002532

715 Poropat, L., Dobslaw, H., Zhang, L., Macrander, A., Boebel, O., & Thomas, M.

(2018). Time variations in ocean bottom pressure from a few hours to many years: In situ data, numerical models, and GRACE satellite gravimetry. *Journal of Geophysical Research: Oceans*, *123*(8), 5612-5623. Retrieved from https://agupubs.onlinelibrary.wiley.com/doi/abs/10.1029/2018JC014108 doi: https://doi.org/10.1029/2018JC014108

Purkey, S. G., & Johnson, G. C. (2012). Global contraction of Antarctic Bottom Water between the 1980s and 2000s. *Journal of Climate*, *25*(17), 5830 - 5844. Retrieved from https://journals.ametsoc.org/view/journals/clim/25/17/jcli-d-11-00612.1.xml doi: 10.1175/JCLI-D-11-00612.1

Sloyan, B. M., & Rintoul, S. R. (2001). The southern ocean limb of the global deep overturning circulation. *Journal of Physical Oceanography*, *31*(1), 143 - 173. Retrieved from https://journals.ametsoc.org/view/journals/phoc/31/1/1520-0485_2001_031_0143_tsolot_2.0.co_2.xml doi: 10.1175/1520-0485(2001)031⟨0143:TSOLOT⟩2.0.CO;2

Solodoch, A., Stewart, A. L., Hogg, A. M., Morrison, A. K., Kiss, A. E., Thompson, A. F., ... Cimoli, L. (2022). How does Antarctic Bottom Water cross the southern ocean? *Geophysical Research Letters*, *n/a*(n/a). Retrieved from https://agupubs.onlinelibrary.wiley.com/doi/abs/10.1029/2021GL097211 doi: https://doi.org/10.1029/2021GL097211

Solodoch, A., Stewart, A. L., McC. Hogg, A., & Manucharyan, G. E. (2023). Machine learning-derived inference of the Meridional Overturning Circulation from satellite-observable variables in an ocean state estimate. *Journal of Advances in Modeling Earth Systems*, *15*(4), e2022MS003370. Retrieved from https://agupubs.onlinelibrary.wiley.com/doi/abs/10.1029/2022MS003370 (e2022MS003370 2022MS003370) doi: https://doi.org/10.1029/2022MS003370

Stewart, A. L., Chi, X., Solodoch, A., & Hogg, A. M. (2021). High-frequency fluctuations in Antarctic Bottom Water transport driven by southern ocean winds. *Geophysical Research Letters*, *48*(17). Retrieved from https://agupubs.onlinelibrary.wiley.com/doi/abs/10.1029/2021GL094569 doi: https://doi.org/10.1029/2021GL094569

Talley, L. D. (2013, March). Closure of the global overturning circulation through the Indian, Pacific, and Southern Oceans: Schematics and transports.

Oceanography. Retrieved from https://doi.org/10.5670/oceanog.2013.07

Tsujino, H., Urakawa, S., Nakano, H., Small, R. J., Kim, W. M., Yeager, S. G., ... Yamazaki, D. (2018, 10). JRA-55 based surface dataset for driving ocean–sea-ice models (JRA55-do). *Ocean Modelling*, *130*. doi: 10.1016/j.ocemod.2018.07.002

Valla, D., Piola, A. R., Meinen, C. S., & Campos, E. (2019). Abyssal transport variations in the southwest South Atlantic: First insights from a long-term observation array at 34.5 °S. *Geophysical Research Letters*, *46*(12), 6699-6705. Retrieved from https://agupubs.onlinelibrary.wiley.com/doi/abs/10.1029/2019GL082740 doi: https://doi.org/10.1029/2019GL082740

Watkins, M. M., Wiese, D. N., Yuan, D.-N., Boening, C., & Landerer, F. W. (2015). Improved methods for observing earth's time variable mass distribution with GRACE using spherical cap mascons. *Journal of Geophysical Research: Solid Earth*, *120*(4), 2648-2671. Retrieved from https://agupubs.onlinelibrary.wiley.com/doi/abs/10.1002/2014JB011547 doi: https://doi.org/10.1002/2014JB011547

Wiese, D. N., Bienstock, B., Blackwood, C., Chrone, J., Loomis, B. D., Sauber, J., ... Zlotnicki, V. (2022). The mass change designated observable study: Overview and results. *Earth and Space Science*, *9*(8), e2022EA002311. Retrieved from https://agupubs.onlinelibrary.wiley.com/doi/abs/10.1029/2022EA002311 (e2022EA002311 2022EA002311) doi: https://doi.org/10.1029/2022EA002311

Zhang, L., Delworth, T. L., Cooke, W., & Yang, X. (2019). Natural variability of southern ocean convection as a driver of observed climate trends. *Nature Climate Change*, *9*(1), 59–65. Retrieved from https://doi.org/10.1038/s41558-018-0350-3 doi: 10.1038/s41558-018-0350-3

Zhou, S., Meijers, A. J. S., Meredith, M. P., Abrahamsen, E. P., Holland, P. R., Silvano, A., ... Østerhus, S. (2023). Slowdown of Antarctic Bottom Water export driven by climatic wind and sea-ice changes. *Nature Climate Change*, *13*(7), 701–709. Retrieved from https://doi.org/10.1038/s41558-023-01695-4 doi: 10.1038/s41558-023-01695-4